

Anisotropy of incommensurate magnetic excitations in slightly overdoped $\text{Ba}_{0.5}\text{K}_{0.5}\text{Fe}_2\text{As}_2$ probed by polarized inelastic neutron scattering experiments

N. Qureshi,^{1,*} C. H. Lee,² K. Kihou,² K. Schmalzl,³ P. Steffens,⁴ and M. Braden^{1,†}

¹*II. Physikalisches Institut, Universität zu Köln, Zùlpicher Strasse 77, D-50937 Köln, Germany*

²*National Institute of Advanced Science and Technology (AIST), Tsukuba, Ibaraki 305-8568, Japan*

³*Jùlich Centre for Neutron Science JCNS, Forschungszentrum Jùlich GmbH,*

Outstation at ILL, BP156, 38042 Grenoble, France)

⁴*Institut Laue Langevin, BP156X, 38042 Grenoble Cedex, France*

(Dated: October 28, 2018)

Polarized neutron scattering experiments on the slightly overdoped superconductor $\text{Ba}_{0.5}\text{K}_{0.5}\text{Fe}_2\text{As}_2$ reveal broad magnetic resonance scattering peaking at approximately 15 meV. In spite of doping far beyond the suppression of magnetic order, this compound exhibits dispersive and anisotropic magnetic excitations. At energies below the resonance maximum, magnetic correlations polarized parallel to the layers but perpendicular to the propagation vector are reduced by a factor two compared to those in the two orthogonal directions; in contrast correlations at the peak maximum are isotropic.

PACS numbers: 74.70.Xa; 75.40.Gb; 78.70.Nx

Keywords:

The observation of enhanced magnetic fluctuations in the superconducting phases of FeAs-based materials¹ yields the strongest support for a pairing mechanism associated with magnetism.² Collective resonance excitations appearing just at the propagation vector of the antiferromagnetic order in the parent phases were reported in polycrystalline optimally hole-doped $\text{Ba}_{0.6}\text{K}_{0.4}\text{Fe}_2\text{As}_2$ (Ref. 2) as well as in the electron-doped BaFe_2As_2 series.^{3,4} Various neutron scattering studies report the effect of electron doping on the resonance peak by substituting Fe by either Co (Refs. 3,5–9) or Ni (Refs. 4,10–13). The energy of this excitation has been found to scale with T_c and the intensity behaves like the superconducting ordering parameter⁴ while the dispersion of the resonance seems to reflect the vicinity of the antiferromagnetic phase.¹⁴ A rather strong resonance has been detected in single-crystalline optimally hole-doped $\text{Ba}_{0.67}\text{K}_{0.33}\text{Fe}_2\text{As}_2$ ($T_c=38$ K).^{15,16}

Using polarized neutron scattering one may distinguish the polarization direction of the fluctuating magnetic moments and thereby directly detect possible spin-space anisotropies of magnetic excitations. Such experiments were performed on Co (Ref. 17), on Ni-doped BaFe_2As_2 (Ref. 18) and on $\text{Ba}_{0.67}\text{K}_{0.33}\text{Fe}_2\text{As}_2$ (Ref. 19) revealing clear evidence for strong spin-space anisotropy with a universal scheme. Scanning the energy dependence of the magnetic scattering at the fixed scattering vector $\mathbf{Q}=(0.5\ 0.5\ q_l)$ yields an isotropic signal just at the maximum of the total scattering. This broad maximum is usually detected in unpolarized neutron scattering experiments and labelled as the resonance mode. At the lower energy side however, magnetic excitations are anisotropic. Anisotropic scattering either appears in form of a sharp isolated peak¹⁷ or just as a shoulder^{18,19} of the broad resonance feature. The three directions relevant for the discussion of the spin-space anisotropy in doped BaFe_2As_4 can be labelled as longitudinal in-plane, i.e. parallel to

the in-plane component of the scattering vector, which we always chose as $\mathbf{Q}=(0.5\ 0.5\ q_l)$, [110], transverse in-plane, i.e. perpendicular to the scattering vector and parallel to the planes $[1\bar{1}0]$, and out of plane. All studies^{17–19} indicate that the transversal in-plane polarized magnetic excitations only appear at higher energies in the superconducting samples and that they do not contribute to the anisotropic signal. This anisotropy, therefore, closely resembles the observation of pure and antiferromagnetic ordered BaFe_2As_2 (Ref. 20). However, so far anisotropic magnetic response has only been reported for superconducting samples close to the antiferromagnetically ordered phase leaving the relevance of this anisotropy for the superconducting state matter of debate.

Here we present a polarized inelastic neutron scattering study on the hole-overdoped compound $\text{Ba}_{0.5}\text{K}_{0.5}\text{Fe}_2\text{As}_2$. Besides their rather high superconducting transition temperatures the K over-doped samples appear interesting as they bridge the superconducting state at optimum doping^{21–23} supposed to exhibit s_{\pm} symmetry with that in KFe_2As_2 ²⁴ for which other order parameter symmetries were proposed.²⁶ Concomitantly, the magnetic response changes from commensurate excitations at $x=0.33$ ^{15,16} to longitudinally modulated ones observed in KFe_2As_2 .²⁵ So far the intermediate doping range was only studied by powder neutron scattering experiments reporting the evolution of the longitudinal incommensurabilities.²⁸ Although the doping level in $\text{Ba}_{0.5}\text{K}_{0.5}\text{Fe}_2\text{As}_2$ is located considerably above the value where antiferromagnetic order fully disappears, we have found that this compound still exhibits signatures of the ordered phase: There is sizeable q_l dispersion and most importantly a well defined spin-space anisotropy develops below the resonance energy.

Single crystals of $\text{Ba}_{0.5}\text{K}_{0.5}\text{Fe}_2\text{As}_2$ were grown by the self-flux method.²⁹ The critical temperature of the single crystals was determined to be 36 K from the temperature

dependence of the zero-field-cooled magnetization studied on several individual single crystals with a SQUID magnetometer. The c lattice constant of each single crystal was examined by x-ray diffraction on both sides of the tabular-shaped samples. We find only minor variation with values staying between 13.40 and 13.45 Å indicating a variation of the K content below $\Delta x = \pm 0.028$. A total number of 60 single crystals with a total mass of 1.3 g were co-aligned on a thin Al sample holder.

Polarized inelastic neutron scattering experiments with longitudinal polarization analysis were carried out at the thermal-beam spectrometers IN20 and IN22 (ILL, Grenoble). Both spectrometers were equipped with polarizing Heusler (111) crystals as monochromator and analyzer. The flipping ratio was determined on a nuclear reflection to be approximately 17 at IN20 and 13 at IN22, respectively. All inelastic scans were performed with a constant \mathbf{k}_f of 2.662 \AA^{-1} . The sample was mounted in the $[110]/[001]$ scattering plane. Longitudinal polarization analysis was performed using the CRYOPAD device to guide and orient the neutron polarization with a strictly zero magnetic field at the sample position in order to avoid errors due to flux inclusion and field repulsion in the superconducting state of the sample. We use the common coordinate system in polarized neutron scattering³⁰ with x pointing along the scattering vector, y being perpendicular to x within the scattering plane, and z pointing perpendicular to the scattering plane. As a general law neutron scattering only senses magnetic excitations polarized perpendicular to the scattering vector \mathbf{Q} . With the polarization analysis it is possible to separate nuclear scattering [always a non-spin-flip (NSF) process] from magnetic scattering and to separate magnetic fluctuations polarized along different direction in spin space. Magnetic excitations contribute to the spin-flip (SF) channel only for magnetic components oscillating perpendicular to the initial polarization axis \mathbf{P}_i . In contrast, magnetic excitations with components oscillating parallel to \mathbf{P}_i are detected in the NSF channel. For each point in the scan the three SF channels and the NSF $_x$ channel have been measured, the latter being a reference for spurious scattering. The respective magnetic cross sections for the in-plane and out-of-plane response, σ_z and σ_y , respectively, can be deduced by simple algebra and by correcting for the finite flipping ratio as it is explained in detail in Ref. 20.

As a first step of the characterization of the magnetic fluctuations in $\text{Ba}_{0.5}\text{K}_{0.5}\text{Fe}_2\text{As}_2$ a longitudinal constant-energy scan was performed at the IN20 spectrometer in order to derive the incommensurability of the magnetic signal. Fig. 1 shows the raw data at an energy transfer of 13 meV for the three SF channels. The longitudinally split peaks are clearly visible in the purely magnetic SF channels. We have derived an incommensurability of $0.083(2)$ reduced lattice units for $E=13 \text{ meV}$ from a fit of a pair of symmetrical Gaussian functions to the SF $_x$ data. The incommensurate character of the scattering and the value of the pitch perfectly agree with the data

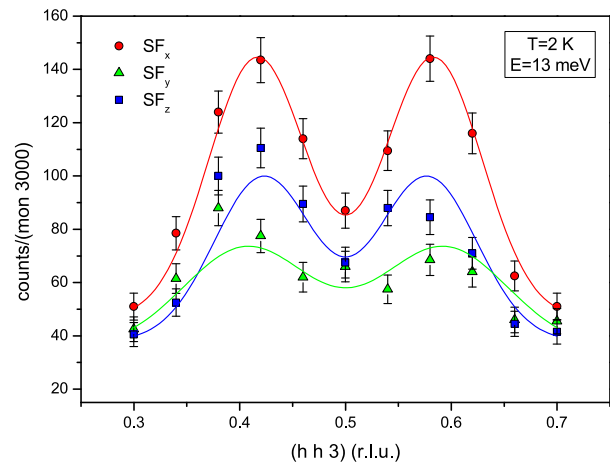


FIG. 1: (Color online) Longitudinal constant-energy scan at $E=13 \text{ meV}$ across $\mathbf{Q}=(0.5 \ 0.5 \ 3)$ (measured at the IN20 spectrometer, monitor 3000 corresponds to 580 s of beam time at $E=13 \text{ meV}$) proving the incommensurability of the magnetic resonance peak.

obtained on powders²⁸ and with our own unpolarized neutron studies²⁷; with the doping the shape of the Fermi surface sheets and therefore the nesting conditions change inducing incommensurate scattering.²⁸ For the energy scans aiming to detect the spin anisotropy we chose the average incommensurability resulting from the unpolarized experiments, i.e. $\mathbf{Q}=(0.56 \ 0.56 \ q_l)$. Fig. 1 shows, furthermore, significant anisotropy with the scattered intensity in the SF $_z$ channel being stronger than that in the SF $_y$ channel. In order to reveal the energy dependence of this anisotropy constant- \mathbf{Q} scans at $\mathbf{Q}=(0.56 \ 0.56 \ 3)$ [Fig. 2(a)-(b)] and at $\mathbf{Q}=(0.56 \ 0.56 \ 2)$ [Fig. 2(c)-(d)] were carried out at $T=2 \text{ K}$ (Note that the data in this and all following figures have been obtained on the IN22 spectrometer, however, the IN20 spectrometer yields the same results). Figs. 2(a) and (c) show the raw data in the SF channels together with a polynomial fit to the SF $_x$ scattering at 40 K. A clear magnetic signal is observable around 15 meV forming the broad magnetic resonance peak as a consequence of the opening of the superconducting gap and the redistribution of spectral weight indicated by the SF $_x$ scattering at $T > T_C$. Figs. 2(b) and (d) show the magnetic cross sections $\sigma_{y,z}$ obtained by subtracting the SF channels following Ref. 20 and by correcting for the finite flipping ratio, the Bose factor and higher order contaminations at the monitor, yielding the imaginary part of the magnetic susceptibility. Similar to previous reports on other FeAs compounds the excitations corresponding to σ_y set in at lower energy than the transverse in-plane ones corresponding to σ_z . Furthermore, the raw data [Figs. 2(a) and (c)] suggest a weak dispersion for both the in-plane and out-of-plane response of the magnetic resonance peak between the scattering vector with odd $q_l=3$ and that with even $q_l=2$. In order to quantify the band width the total magnetic signal $(\text{SF}_x + \text{SF}_y + \text{SF}_z)/2$

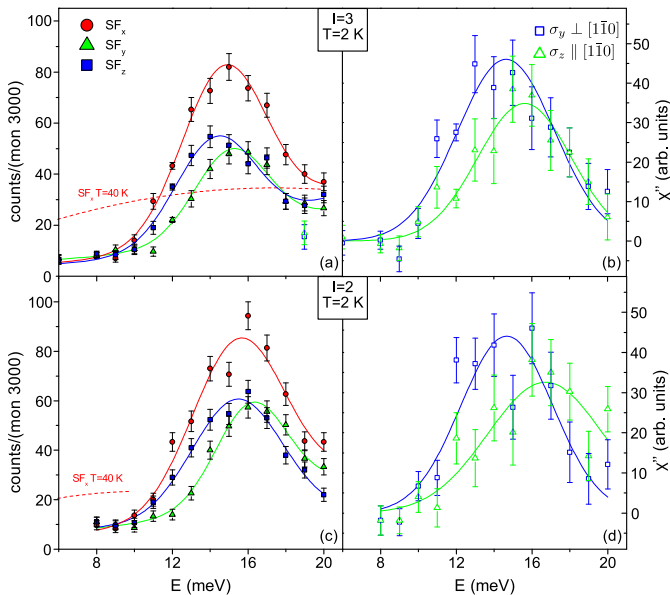


FIG. 2: (Color online) Constant- q scans at $\mathbf{Q}=(0.56\ 0.56\ 3)$ (first row) and $\mathbf{Q}=(0.56\ 0.56\ 2)$ (second row) at 2 K within the superconducting phase (measured at the IN22 spectrometer). (a) and (c) show the raw intensities of the SF channels together with the SF_x scattering at $T=40$ K [(red) dashed line]. The fit of a Gaussian function on a second degree polynomial background to the raw data is represented by solid lines. In (b) and (d) the imaginary part of the magnetic susceptibility is depicted after correcting the raw intensities as described in the text. The solid lines are Gaussian fits on a zero background (monitor 3000 corresponds to 530 s of beam time at $E=8$ meV and 680 s at $E=20$ meV on IN22, this also applies to figures 3-5).

has been analyzed which is shown in Fig. 3. From the fit of a Gaussian function on a polynomial background to the total magnetic signal with $q_l=3$ and $q_l=2$ we have derived a band width of approximately 1 meV, see also Ref. 27

In order to prove that the spin-space anisotropy is connected to the superconducting state we have followed the scattered intensity at $\mathbf{Q}=(0.56\ 0.56\ 3)$ and an energy transfer of 12 meV, where according to Fig. 2(a) a pronounced anisotropy is present, as a function of temperature. Fig. 4 shows the scattering in the two SF channels. No difference within the error bars is visible above T_c (indicated by the dashed line) indicating an isotropic system. At cooling below T_c a significant spin-space anisotropy emerges.

The polarization analysis directly distinguishes between σ_z always sensing the transversal in-plane magnetic contributions and σ_y sensing the fluctuations parallel to the neutron scattering plane. Further information can be obtained by varying the scattering vector $\mathbf{Q}=(0.56, 0.56, q_l)$: For $q_l=0$ only out-of-plane fluctuations can contribute to σ_y , but this out-of-plane contribution

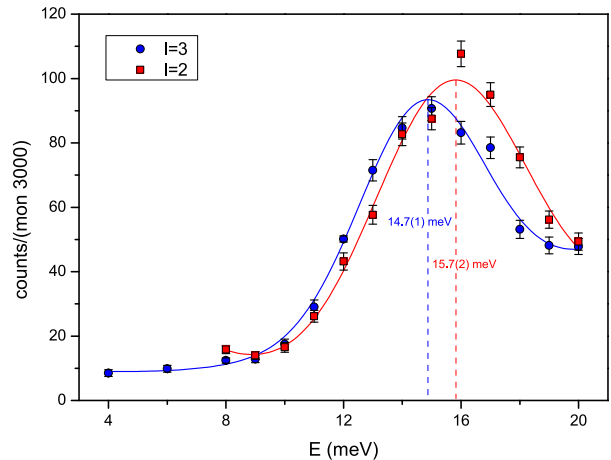


FIG. 3: (Color online) Total magnetic intensity obtained by $(SF_x+SF_y+SF_z)/2$ indicating a weakly dispersive magnetic resonance peak. The solid lines are Gaussian functions on a second degree polynomial background fitted to the raw data. From the peak positions a bandwidth of 1 meV can be obtained (errors given in brackets correspond to the preceding digit).

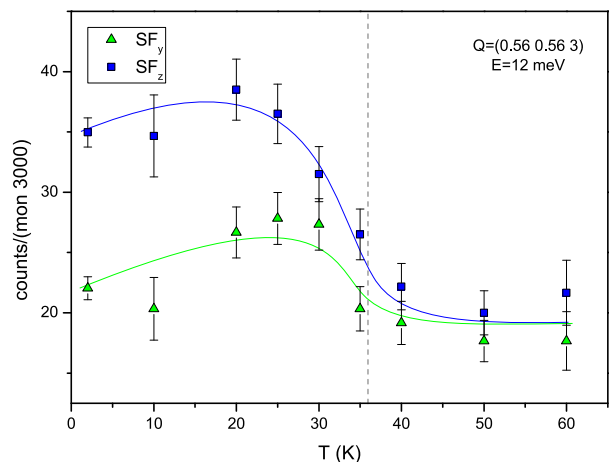


FIG. 4: (Color online) Peak intensity of the magnetic scattering at $\mathbf{Q}=(0.56\ 0.56\ 3)$ and $E=12$ meV as a function of temperature. A clear splitting of the in-plane (SF_y) and the out-of-plane (SF_z) components is visible at T_c which is indicated by the dashed line. The solid lines are guides to the eye.

decreases with increasing q_l while the in-plane longitudinal contribution increases with the geometry factor $\sin(\alpha)^2 = \left(\frac{q_l}{|\mathbf{Q}|}\right)^2$ (q -components given in absolute units here; α the angle between $[110]$ and the scattering vector \mathbf{Q}). Fig. 5 shows the magnetic signal at $\mathbf{Q}=(0.56\ 0.56\ q_l)$ for odd q_l values up to 5. Fig. 5(a) clearly reveals the anisotropy which we have observed at $E=12$ meV up to $q_l=5$. In contrast, Fig. 5(c) and the inset of Fig. 5(a) confirm the isotropic fluctuations at an energy transfer of 15 meV and above T_c , respectively. In order to analyze the respective intensities quantitatively we have con-

verted the raw data to the imaginary part of the magnetic susceptibility [see Fig. 5(b)]. Let us first consider the magnetic cross section σ_z measured in the SF_y channel, which is not subject to the geometrical factor with varying q_l value. Therefore, an increase in q_l will affect the intensities by the magnetic form factor $f(\mathbf{Q})$ only. In fact, σ_z is reduced proportional to $f(\mathbf{Q})^2$ which is shown by the (green) dash-dotted line normalized to $\sigma_z(q_l=1)$. As mentioned above, the out-of-plane contributions in the SF_z channel are reduced by an increasing q_l value, therefore, the (blue) dashed line represents $f(\mathbf{Q})^2 \cos^2 \alpha$, with α the angle between \mathbf{Q} and the [110] direction, normalized to the data point $\sigma_y(q_l=1)$. It becomes evident that a purely out-of-plane fluctuation is reduced more severely, but our data still shows $\sigma_y > \sigma_z$ at $q_l=5$. Such a behavior can only be explained by a sizeable in-plane longitudinal contribution of magnetic fluctuations. We have fitted the 12 meV data with $f(\mathbf{Q})^2 [n_t \cos^2 \alpha + (1 - n_t) \sin^2 \alpha]$ normalized to the intensity at $l = 1$, where n_t defines the fraction of the σ_y channel intensity which stems from the out-of-plane fluctuation. The fit reveals a value of $n_t=0.53(7)$ stating that the in-plane longitudinal fluctuation is of comparable strength as the out-of-plane fluctuation. On the contrary, at this energy of 12 meV the transversal in-plane fluctuations are reduced by roughly a factor two. Transversal in-plane magnetic fluctuations seem to appear at higher energy. Therefore, the character of the magnetic correlations in Ba_{0.5}K_{0.5}Fe₂As₂ can be considered as an easy-plane type (two soft and one hard axes). Spin orbit coupling is clearly a relevant parameter for a quantitative understanding of magnetic excitations in superconducting FeAs-based compounds even when they are not close to the antiferromagnetic phase. Fig. 5(d) shows that there seems to be no anisotropy in the spin excitations at 15meV, whose q_l dependence is well described by the magnetic form factor.

In conclusion we have presented inelastic neutron scattering data with longitudinal polarization analysis revealing anisotropic and dispersive magnetic excitations in superconducting Ba_{0.5}K_{0.5}Fe₂As₂. The investigated sample is in the overdoped region of the phase diagram²³ and therefore far away from the magnetically ordered phase. Nevertheless the anisotropic magnetic character of the parent compound²⁰ persists as we find c polarized spin fluctuations at lower energies than the transverse in-plane polarized modes. Spin space anisotropy induced by spin-orbit coupling is thus relevant in a broad part of the superconducting phase and not only near the existence of static antiferromagnetic order. By analyzing the q_l dependence of magnetic excitations we can furthermore identify pronounced in-plane anisotropy. Magnetic correlations in Ba_{0.5}K_{0.5}Fe₂As₂ exhibit an easy-plane or hard-axis character, like it is the case for electron

doping.^{17,18,31} This magnetic anisotropy must arise from spin orbit coupling and a peculiar orbital arrangement. Furthermore, in light of the universality of the dispersive spin-resonance mode among the FeAs superconductors,¹⁴ Ba_{0.5}K_{0.5}Fe₂As₂ exhibits significant q_l dispersion of the

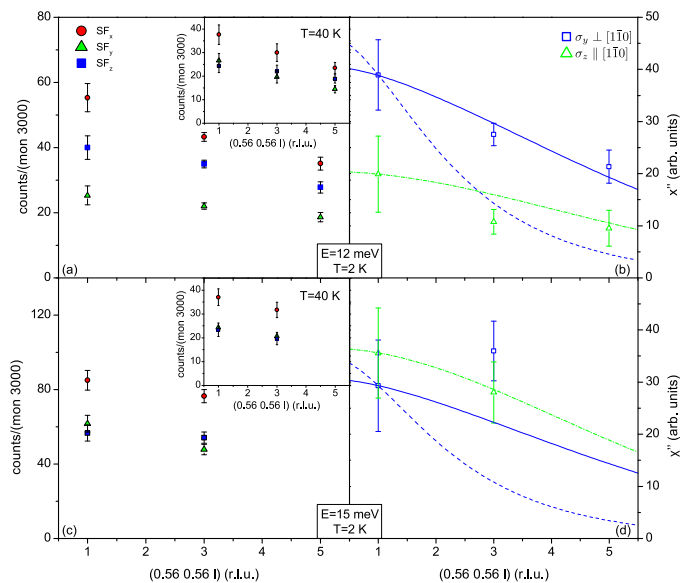


FIG. 5: (Color online) q_l dependence of the magnetic signal at $\mathbf{Q}=(0.56 \ 0.56 \ q_l)$ and $T=2$ K for an energy transfer of 12 meV (first row) and 15 meV (second row). (a) and (c) show the raw intensities of the SF channels (the insets show the data at $T=40$ K). (b) and (d) show the magnetic cross sections $\sigma_{y,z}$. The (green) dash-dotted line in (b) represents the magnetic form factor normalized to the σ_z data point at $q_l=1$, the (blue) dashed line is the geometrical factor (only containing the transversal component of the fluctuation) times the magnetic form factor normalized to the σ_y data point at $q_l=1$ and the (blue) solid line is a fit containing the geometrical factor (both the longitudinal and the transversal part of the fluctuation) times the magnetic form factor normalized in the same way. In (d) the (blue) solid line shows the fit in (b) adjusted to the σ_y $q_l=1$ point due to the small extent in q_l range.

magnetic resonance.

Acknowledgments

This study was supported by a Grant-in-Aid for Scientific Research B (No. 24340090) from the Japan Society for the Promotion of Science and by the Deutsche Forschungsgemeinschaft through the Priority Programme SPP1458 (Grant No. BR2211/1-1).

* Corresponding author. Electronic address: qureshi@ph2.uni-koeln.de

† Electronic address: braden@ph2.uni-koeln.de

¹ Y. Kamihara, T. Watanabe, M. Hirano, and H. Hosono, J.

- Am. Chem. Soc. **130**, 3296 (2008).
- ² A. D. Christianson, E. A. Goremychkin, R. Osborn, S. Rosenkranz, M. D. Lumsden, C. D. Malliakas, I. S. Todorov, H. Claus, D. Y. Chung, M. G. Kanatzidis, et al., *Nature* **456**, 930 (2008), nature.
 - ³ M. D. Lumsden, A. D. Christianson, D. Parshall, M. B. Stone, S. E. Nagler, G. J. MacDougall, H. A. Mook, K. Lokshin, T. Egami, D. L. Abernathy, et al., *Phys. Rev. Lett.* **102**, 107005 (2009).
 - ⁴ S. Chi, A. Schneidewind, J. Zhao, L. W. Harriger, L. Li, Y. Luo, G. Cao, Z. Xu, M. Loewenhaupt, J. Hu, et al., *Phys. Rev. Lett.* **102**, 107006 (2009).
 - ⁵ D. Parshall, K. A. Lokshin, J. Niedziela, A. D. Christianson, M. D. Lumsden, H. A. Mook, S. E. Nagler, M. A. McGuire, M. B. Stone, D. L. Abernathy, et al., *Phys. Rev. B* **80**, 012502 (2009).
 - ⁶ D. S. Inosov, J. T. Park, P. Bourges, D. L. Sun, Y. Sidis, A. Schneidewind, K. Hradil, D. haug, C. T. Lin, B. Keimer, et al., *Nature Phys.* **6**, 178 (2010).
 - ⁷ D. K. Pratt, A. Kreyssig, S. Nandi, N. Ni, A. Thaler, M. D. Lumsden, W. Tian, J. L. Zarestky, S. L. Bud'ko, P. C. Canfield, et al., *Phys. Rev. B* **81**, 140510(R) (2010).
 - ⁸ J. T. Park, D. S. Inosov, A. Yaresko, S. Graser, D. L. Sun, P. Bourges, Y. Sidis, Y. Li, J.-H. Kim, D. Haug, et al., *Phys. Rev. B* **82**, 134503 (2010).
 - ⁹ H.-F. Li, C. Broholm, D. Vaknin, R. M. Fernandes, D. L. Abernathy, M. B. Stone, D. K. Pratt, W. Tian, Y. Qiu, N. Ni, et al., *Phys. Rev. B* **82**, 140503(R) (2010).
 - ¹⁰ S. Li, Y. Chen, S. Chang, J. W. Lynn, L. Li, Y. Luo, G. Cao, Z. Xu, and P. Dai, *Phys. Rev. B* **79**, 174527 (2009).
 - ¹¹ L. W. Harriger, A. Schneidewind, S. Li, J. Zhao, Z. Li, W. Lu, X. Dong, F. Zhou, Z. Zhao, J. Hu, et al., *Phys. Rev. Lett.* **103**, 087005 (2009).
 - ¹² O. J. Lipscombe, L. W. Harriger, P. G. Freeman, M. Enderle, C. Zhang, M. Wang, T. Egami, J. Hu, T. Xiang, M. R. Norman, et al., *Phys. Rev. B* **82**, 064515 (2010).
 - ¹³ M. Wang, H. Luo, M. Wang, S. Chi, J. A. Rodriguez-Rivera, D. Singh, S. Chang, J. W. Lynn, and P. Dai, *Phys. Rev. B* **83**, 094516 (2011).
 - ¹⁴ C. H. Lee, P. Steffens, N. Qureshi, M. Nakajima, K. Kihou, A. Iyo, H. Eisaki, and M. Braden, *Phys. Rev. Lett.* **111**, 167002 (2013).
 - ¹⁵ M. Wang, et al., *Nat. Commun.* **4**:2874 doi: 10.1038/ncomms3874 (2013).
 - ¹⁶ C. L. Zhang et al., *Sci. Rep.* **1**, 115 (2011).
 - ¹⁷ P. Steffens, C. H. Lee, N. Qureshi, K. Kihou, A. Iyo, H. Eisaki, and M. Braden, *Phys. Rev. Lett.* **110**, 137001 (2013).
 - ¹⁸ H. Luo, M. Wang, C. Zhang, X. Lu, L.-P. Regnault, R. Zhang, S. Li, J. Hu and P.-C. Dai. *Phys. Rev. Lett.* **111**, 107006 (2013).
 - ¹⁹ C. Zhang, M. Liu, Y. Su, L.-P. Regnault, M. Wang, G. Tan, T. Brückel, T. Egami, and P. Dai, *Phys. Rev. B* **87**, 081101(R) (2013).
 - ²⁰ N. Qureshi, P. Steffens, S. Wurmehl, S. Aswartham, B. Büchner, and M. Braden, *Phys. Rev. B* **86**, 060410(R) (2012).
 - ²¹ M. Rotter, M. Tegel, and D. Johrendt, *Phys. Rev. Lett.* **101**, 107006 (2008).
 - ²² R. R. Urbano, E. L. Green, W. G. Moulton, A. P. Reyes, P. L. Kuhns, E. M. Bittar, C. Adriano, T. M. Garitezi, L. Bufaiçal, and P. G. Pagliuso, *Phys. Rev. Lett.* **105**, 107001 (2010).
 - ²³ S. Avci, O. Chmaissem, D. Y. Chung, S. Rosenkranz, E. A. Goremychkin, J. P. Castellan, I. S. Todorov, J. A. Schlueter, H. Claus, A. Daoud-Aladine, et al., *Phys. Rev. B* **85**, 184507 (2012).
 - ²⁴ C. Liu, G. D. Samolyuk, Y. Lee, N. Ni, T. Kondo, A. F. Santander-Syro, S. L. Bud'ko, J. L. McChesney, E. Rotenberg, T. Valla, et al., *Phys. Rev. Lett.* **101**, 177005 (2008).
 - ²⁵ C. H. Lee, K. Kihou, H. Kawano-Furukawa, T. Saito, A. Iyo, H. Eisaki, H. Fukazawa, Y. Kohori, K. Suzuki, H. Usui, K. Kuroki, and K. Yamada *Phys. Rev. Lett.* **106**, 067003 (2011).
 - ²⁶ J.-Ph. Reid, M. A. Tanatar, A. Juneau-Fecteau, R. T. Gordon, S. R. de Cotret, N. Doiron-Leyraud, T. Saito, H. Fukazawa, Y. Kohori, K. Kihou, C. H. Lee, A. Iyo, H. Eisaki, R. Prozorov, and Louis Taillefer, *Phys. Rev. Lett.* **109**, 087001 (2012).
 - ²⁷ C. H. Lee et al., unpublished results.
 - ²⁸ J.-P. Castellan, S. Rosenkranz, E. A. Goremychkin, D. Y. Chung, I. S. Todorov, M. G. Kanatzidis, I. Eremin, J. Knolle, A. V. Chubukov, S. Maiti, et al., *Phys. Rev. Lett.* **107**, 177003 (2011).
 - ²⁹ K. Kihou, T. Saito, S. Ishida, M. Nakajima, Y. Tomioka, H. Fukazawa, Y. Kohori, T. Ito, S. Uchida, A. Iyo, et al., *J. Phys. Soc. Jpn.* **79**, 124713 (2010).
 - ³⁰ P.J. Brown, *Spherical Neutron Polarimetry*, in *Neutron Scattering from Magnetic Materials*, Edt. T. Chatterji, Elsevier B.V. (2006).
 - ³¹ F. Waßer, A. Schneidewind, Y. Sidis, S. Aswartham, S. Wurmehl, B. Büchner, and M. Braden, arXiv1407.1417 (2014).